AIAA JOURNAL
Vol. 42, No. 9, September 2004

Empirical Spectral Model of Surface Pressure Fluctuations

Michael Goody*
U.S. Naval Surface Warfare Center, West Bethesda, Maryland 20817-5700

An empirical model of the surface pressure spectrum beneath a two-dimensional, zero-pressure-gradient boundary layer is presented that is based on the experimental surface pressure spectra measured by seven research groups. The measurements cover a large range of Reynolds number, $1.4 \times 10^3 < Re_\theta < 2.34 \times 10^4$. The model is a simple function of the ratio of the timescales of the outer to inner boundary layer. It incorporates the effect of Reynolds number through the timescale ratio and compares well to experimental data. It is proposed that the effect of Reynolds number is more aptly described as the effect of the range of relevant scales. Spectral features of the experimental data and the scaling behavior of the surface pressure spectrum are also discussed.

Nomenclature

C_f = skin friction coefficient, τ_w/Q_e
d = sensing diameter of the pressure transducer
d^+ = d normalized by the viscous length scale, $u_\tau d/\nu$
p = unsteady pressure (mean zero) due to turbulence
$\overline{p^2}$ = mean square unsteady pressure
Q_e = dynamic pressure at the boundary-layer edge
Re_θ = momentum Reynolds number, $U_e\theta/\nu$
R_T = ratio of timescales of p [Eq. (3)]
U = magnitude of the flow velocity
U_c = convection velocity of p
U_e = velocity at the boundary-layer edge
u_τ = friction velocity, $(\tau_w/\rho)^{1/2}$
δ = boundary-layer thickness
δ^* = boundary-layer displacement thickness
θ = boundary-layer momentum thickness
μ = dynamic viscosity of fluid
ν = kinematic viscosity, μ/ρ
ρ = mass density of fluid
τ_w = shear stress at the wall
Φ = spectral power density of surface pressure fluctuations such that (single-sided)

$$\overline{p^2} = \int_0^\infty \Phi(\omega)\,\mathrm{d}\omega$$

ω = angular frequency

I. Introduction

A. Boundary-Layer Scaling: General

SCALING is a technique that is often used in the analysis of boundary layers. It is based on the concept of self-similarity, in which a function of some variable(s) retains the same shape for a wide variety of conditions. If self-similar, a dependent variable can be made nondimensional by appropriate length, velocity, and/or pressure scales and expressed as a universal function of independent variable(s) that are also made nondimensional on appropriate length, velocity, and/or pressure scales.[1,2] The function is called universal because it does not change for a wide variety of conditions.

The application of self-similarity to the analysis of turbulent boundary layers is more complicated. One characteristic of turbulent boundary layers is the large range of relevant length, velocity, and pressure scales. The different boundary-layer scales are related to organized motions or coherent structures[3,4] that exist in the boundary layer. Traditionally, a two-layer model has been used to scale the turbulent boundary layer.[5] The flow nearest the wall (known as the inner layer) has a set of length, velocity, and pressure scales associated with it. The flow away from the wall (known as the outer layer and consisting of most of the boundary layer) has a different set of length, velocity, and pressure scales associated with it.

The situation is complicated even further when the effect of Reynolds number is considered (see Refs. 6 and 7). The Reynolds number is the ratio of inertial to viscous forces in the boundary layer. Most practical flows, that is, the flow over airplanes and ships, have a large Reynolds number ($Re_\theta \sim 10^5$–10^6). Most laboratory flows, that is, wind tunnels and water tunnels, have a smaller Reynolds number ($Re_\theta \sim 10^3$–10^4). Therefore, understanding the effect of Reynolds number is crucial when applying laboratory results to the analysis of practical flows.

Recently, Buschmann and Gad-el-Hak[8] extended the analysis of Afzal[9] to relate changes in the mean velocity profile with Reynolds number to the change in the ratio of inner-to-outer length scale, $u_\tau\delta/\nu$. Although conceived independently of Buschmann and Gad-el-Hak, the present empirical model is based on a similar precept, namely, that Reynolds number affects the surface pressure spectrum through the ratio of outer-to-inner timescale: the timescale ratio R_T. The timescale ratio increases as the Reynolds number increases.

B. Scaling the Surface Pressure Spectrum

There is no universal scaling that collapses the p spectra beneath flows with different Reynolds number at all frequencies. Traditionally, the two-layer model is applied to pressure fluctuations by using different scales to collapse the p spectrum in specific frequency ranges. The high-frequency end of the p spectra collapse to a significant degree when normalized using inner-layer scales, τ_w as the pressure scale and ν/u_τ^2 as the timescale, and the spectrum decays as ω^{-5} (Fig. 1). There is general agreement in the literature on the proper pressure scales and timescales for the p spectrum at high frequencies. The same is not true for the p spectrum in the low- and middle-frequency ranges. Researchers[10,11] have shown p spectra that collapse at low frequencies using an outer-layer scaling of either τ_w or Q_e as the pressure scale and δ^*/U_e as the timescale. Some researchers refer to the scale combination τ_w and δ^*/U_e as a mixed scaling. Farabee and Casarella[12] reported that Q_e and δ^*/U_e only collapse p spectra at very low frequencies, $\omega\delta^*/U_e \leq 0.03$, and that the spectrum increases as ω^2 in this frequency range, which is in agreement with the theoretical results of others.[10,13] Some researchers[12,14,15] have used τ_w as the pressure scale and δ/u_τ as the timescale to collapse p spectra at middle frequencies. Goody[16] reviewed the experimental p spectra of six research groups that cover

Presented as Paper 2002-2565 at the AIAA/CEAS 8th Aeroacoustics Conference, Breckenridge, CO, 17–19 June 2002; received 18 September 2002; accepted for publication 17 February 2004.

*Mechanical Engineer, Code 7250, Signatures Directorate, Carderock Division. Member AIAA.

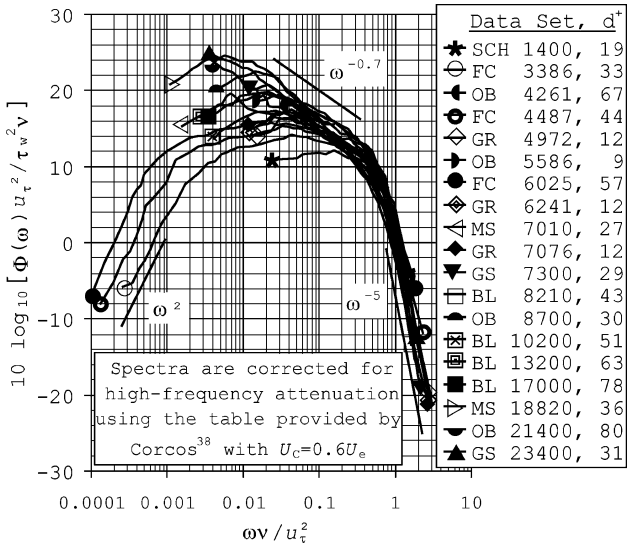

Fig. 1 Experimental p spectra scaled by inner variables: τ_w as pressure scale and ν/u_τ^2 as timescale.

a large Reynolds number range ($1.4 \times 10^3 < Re_\theta < 2.34 \times 10^4$) and showed that the spectra collapse at low and middle frequencies when τ_w is used as the pressure scale and either δ^*/U_e, δ/U_e, δ^*/u_τ, or δ/u_τ is used as the timescale.

It has been postulated,[10,13,17] using arguments related to the existence of an inner scaling and an outer scaling, that an overlap range exists in the p spectrum beneath two-dimensional boundary layers at high Reynolds number. Both inner- and outer-layer scaling collapse the p spectrum in the overlap range. Theoretically,[10,13,17] it is argued that the p spectrum in this frequency range decreases as ω^{-1} and is due to universal turbulent motions within the log-layer where the convection velocity of turbulent structures approaches the local mean flow velocity. However, the measured spectral decay is closer to from $\omega^{-0.7}$ to $\omega^{-0.8}$. For example, McGrath and Simpson[18] measured an $\omega^{-0.7}$ decay, Blake[19] measured an $\omega^{-0.75}$ decay, and Goody and Simpson[20] measured an $\omega^{-0.8}$ decay within the overlap region. Both theoretical and experimental results show that the size/existence of the overlap frequency range increases with Reynolds number. The low Reynolds number ($Re_\theta = 1.4 \times 10^3$) data of Schewe[21] only tangentially approach a power law spectral decay within the overlap range.

C. Spectral Models of the Pressure Spectrum

Howe[22] gives the following model for $\Phi(\omega)$ and attributes it to Chase[23]:

$$\frac{\Phi(\omega)U_e}{\tau_w^2\delta^*} = \frac{2\left(\omega\delta^*/U_e\right)^2}{\left[\left(\omega\delta^*/U_e\right)^2 + 0.0144\right]^{\frac{3}{2}}} \tag{1}$$

Equation (1) is here referred to as the Chase–Howe model. At low frequencies, the model spectrum is proportional to ω^2 and at higher frequencies it varies as ω^{-1}, both of which are consistent with theoretical results. However, Eq. (1) does not include an ω^{-5} spectral decay, which has been measured and theoretically shown to exist at the highest frequencies. The multiplicative constant in the numerator, 2, of Eq. (1) is not in the equation given by Howe,[22] which describes a double-sided spectrum. The constant is used here to make Eq. (1) consistent with the definition of Φ used here (single sided).

Equation (1) is a simplification of Chase's model.[23] The model proposed by Chase is a more comprehensive model for the wave vector–frequency p spectrum. It is by no means the only spectral model of p. Graham[24] discussed the wave vector–frequency spectral models of Corcos,[25] Efimtsov,[26] Smol'yakov and Tkachenko,[27] Chase,[23] and Ffowcs Williams[28] (as approximated by Hwang and Geib[29]) with regard to their ability to predict accurately the modal excitation of a simply supported, thin, elastic plate by calculating the radiated sound. Other notable spectral models are those of Witting[30] and Panton and Robert.[31] The spectral models mentioned are based on the theoretical formulations of either Lighthill[32,33] or Kraichnan.[34] Lighthill[32,33] expressed the momentum equation governing fluid flow in the form of a wave equation, known as acoustic analogy. Kraichnan[34] expressed p as a Poisson equation by taking the divergence of the momentum equation that governs fluid flow. Though based on theoretical formulations, each of the cited spectral models still rely on empirical data at various points in their development to varying degrees of sophistication.

Equation (1) was used as the starting point for the present empirical model because of its attractive functional form. It is able to describe the essential features of the frequency spectrum of p with limited degrees of freedom (adjustable constants). Thus, it is more closely related to the observed scaling behavior than a simple polynomial curve fit, but less complex than a more general model for the wave number–frequency p spectrum.

II. Experimental Data

A. Data Review

All of the experimental p spectra presented here are two-dimensional, zero-pressure-gradient flows. The p spectra of Farabee and Casarella,[12] Olivero-Bally et al.,[14] McGrath and Simpson,[18] and Blake[19] were multiplied by two to be consistent with the definition of Φ used here. The data of McGrath and Simpson[18] presented here is an unpublished rereduction of the original data that was performed by Shinpaugh and Simpson and corrected for the low-frequency response (< 100 Hz) of their transducer.

Some relevant flow conditions for each of the data sets is given in Table 1. Spectral characteristics of each of the data sets are given in Table 2. Each of the data sets included in the present analysis addressed the two main measurement issues concerning the p spectrum.[16] At low frequencies, the measured p spectrum can be contaminated by facility-related, background noise. The data sets included presently either used an acoustically quiet wind tunnel or employed a noise cancellation technique[35–37] to correct the measured p spectrum. Farabee and Casarella[12] used both an acoustically quiet wind tunnel and a noise cancellation technique and were able to measure the p spectrum at frequencies over an order of magnitude lower than any of the other investigations considered here or found elsewhere in the literature. The p spectrum measured by Farabee and Casarella[12] is the only measured p spectrum that could be found in the literature that extends to frequencies that are low enough to exhibit a spectral increase proportional to ω^2.

At high frequencies, spectral levels are attenuated due to the nonzero, finite size of the pressure transducer used. Contributions to p from sources (coherent structures) that are smaller than the transducer sensing area are spatially integrated and, thereby, attenuated because they have zero mean (by definition of p) (Refs. 38–41). Typically, the transducer sensing diameter, scaled on inner-layer variables, $d^+ = u_\tau d/\nu$, is used to characterize whether the attenuation is significant. Schewe[21] reports that $d^+ < 19$ is adequate to resolve the high frequency p. Gravante et al.[15] report that $12 < d^+ < 18$ is required. The transducer size for the present data sets is in the range $9 < d^+ < 80$ (Table 1). Corcos[38] provides an attenuation table in the form

$$\frac{\Phi(\omega)_{\text{measured}}}{\Phi(\omega)_{\text{true}}}$$

as a function of $\omega r/U_c$, where r is the sensing radius for a circular transducer. Others[21,42–44] have verified that the table provided by Corcos[38] accurately recovers the true high-frequency spectral values for $\omega r/U_c < 4$. The data sets included presently were measured using among the smallest transducers of data reported in the literature. For all of the present data sets, $\omega r/U_c < 4$. None of the data sets included presently were corrected for high-frequency attenuation when published. Therefore, all of the data sets (except that of Goody and Simpson[20]) have been corrected for high-frequency attenuation here, using the attenuation table provided by Corcos[38] and assuming that $U_c = 0.6U_e$.

Table 1 Relevant experimental parameters for each data sets

Reference[a]	Fluid	BL scale ratio		Low frequency[b]	High frequency[b]		
						3-dB attenuation[c]	
		Time R_T	Pressure C_f		d^+	$\omega\delta/U_e$	$\omega\nu/u_\tau^2$
Blake[19]							
BL 8210	Air	94.71	0.00293	AWT[d]	43	65.1	0.69
BL 10200		104.12	0.00274		51	61.7	0.59
BL 13200		120.70	0.00245		63	61.2	0.51
BL 17000		138.02	0.00218		78	60.1	0.44
Farabee and Casarella[12]							
FC 3386	Air	47.11	0.00325	AWT	33	39.8	0.85
FC 4487		60.02	0.00306	NC[e]	44	39.1	0.65
FC 6025		76.18	0.00287		57	39.7	0.52
Gravante et al.[15]							
GR 4972	Air	63.12	0.00273	NC	12	159	2.52
GR 6241		73.23	0.00264		12	191	2.61
GR 7076		87.69	0.00278		12	223	2.54
Goody and Simpson[20]							
GS 7300	Air	81.99	0.00262	NC	29	——	——
GS 23400		274.02	0.00217		31	——	——
McGrath and Simpson[18]							
MS 7010	Air	86.44	0.00280	NC	27	97.4	1.11
MS 18820		186.04	0.00226		36	179	0.95
Olivero-Bally et al.[14]							
OB 4261	Air	65.92	0.00323	NC	10	194	2.92
OB 5586		80.53	0.00300		9	258	3.17
OB 8700	H_2O	192.91	0.00322	NC	30	187	0.95
OB 21400		371.56	0.00253		80	149	0.40
Schewe[21]							
SCH 1400	Air	24.69	0.00395	AWT	19	33.8	1.37

[a]Each data set name is constructed using a unique letter combination that denotes the reference and a number that corresponds to the Reynolds number Re_θ of the data set.
[b]Measurement issues.
[c]Calculated using the attenuated power table of Corcos[38] and assuming that $U_C = 0.6U_e$.
[d]Acoustic wind tunnel used.
[e]Noise cancellation employed.

Table 2 Selected spectral features of each of the data sets

Reference	Measurement range		$[\Phi(\omega)U_e/\tau_w^2\delta]_{\max}$		$[\Phi(\omega)u_\tau^2/\tau_w^2\nu]$(dB), $\omega\nu/u_\tau^2 = 1$	
	$\omega\delta/U_e$	$\omega\nu/u_\tau^2$	dB	$\omega\delta/U_e$	Published	Corrected[a]
Blake[19]						
BL 8210	1.1–156	0.0011–2.2	−4	1.5–4.0	−6.6	−1.8
BL 10200	0.42–172	0.0041–1.7	−3	1.5–3.0	−5.1	0.7
BL 13200	0.41–139	0.0034–1.2	−1	2.0	−5.1	2.1
BL 17000	0.38–22	0.0027–0.2	−2	1.0–4.0	——[b]	——[b]
Farabee and Casarella[12]						
FC 3386	0.012–116	0.00026–2.5	−3	1.0–3.0	−2.7	1.0
FC 4487	0.0078–139	0.00013–2.3	−3	1.0–3.0	−1.7	3.4
FC 6025	0.0076–152	0.00010–2.0	−2	1.0–3.0	−4.1	2.8
Gravante et al.[15]						
GR 4972	0.74–185	0.012–2.9	−2	2.0–4.0	0.3	1.4
GR 6241	1.09–208	0.015–2.8	−2	1.5–5.0	−1.5	−0.4
GR 7076	0.96–251	0.011–2.9	−2	2.0–5.0	−3.3	−2.2
Goody and Simpson[20]						
GS 7300	0.90–177	0.0011–2.2	——[b]	——[b]	−1.4	−1.4
GS 23400	0.93–525	0.0034–1.9	——[b]	——[b]	1.9	1.9
McGrath and Simpson[18]						
MS 7010	0.13–115	0.0015–1.3	0	0.5–0.7	−2.7	0.0
MS 18820	0.20–159	0.0011–0.85	1	0.5–0.8	——[b]	——[b]
Olivero-Bally et al.[14]						
OB 4261	2.4–100	0.036–1.5	——[b]	——[b]	2.5	3.5
OB 5586	1.2–115	0.014–1.4	0	1.5–4.0	1.6	2.5
OB 8700	0.79–157	0.0041–0.81	0	2.0–4.0	——[b]	——[b]
OB 21400	1.4–176	0.0038–0.47	−1	1.5–4.0	——[b]	——[b]
Schewe[21]						
SCH 1400	0.56–37	0.0023–1.5	−2	1.0–4.0	2.6	4.7

[a]Calculated using the attenuated power table of Corcos[38] and assuming that $U_C = 0.6U_e$.
[b]Missing entries indicate that the spectral feature could not be ascertained from the data set.

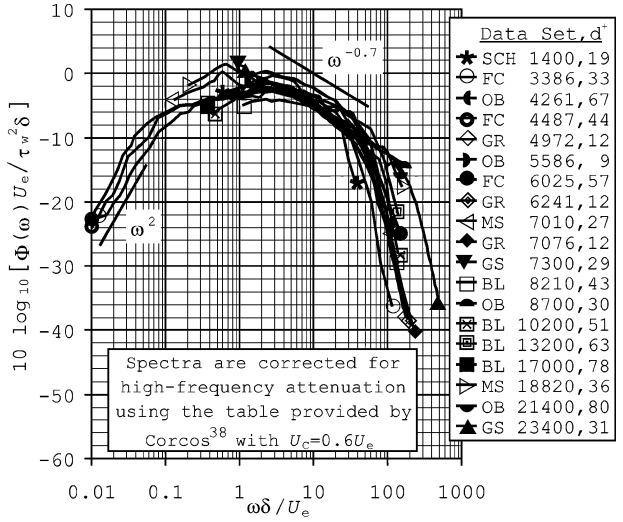

Fig. 2 Experimental p spectra scaled by outer variables: τ_w as pressure scale and δ/U_e as timescale.

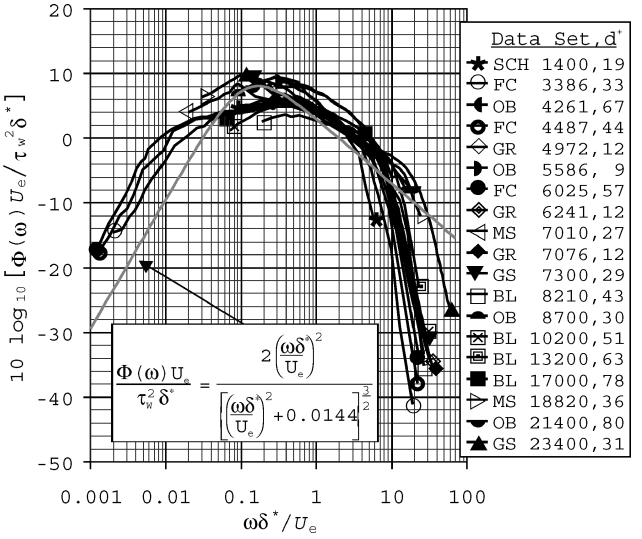

Fig. 3 Experimental p spectra scaled by outer variables: τ_w as pressure scale and δ^*/U_e as timescale.

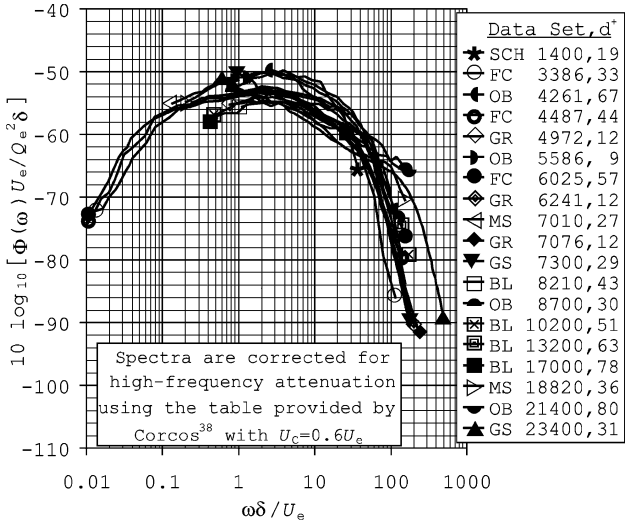

Fig. 4 Experimental p spectra scaled by outer variables: Q_e as pressure scale and δ/U_e as timescale.

Goody and Simpson[20] used a pinhole mask to decrease the effective transducer sensing area. The pinhole mask/transducer system behaves like a Helmholtz resonator, which has a second-order frequency response function. When such a system is used to measure the p spectrum, the frequency response of the pinhole mask/transducer system amplifies the measured p spectrum near the Helmholtz resonant frequency. For the data set of Goody and Simpson, the amplification due to the pinhole mask/transducer frequency response was nearly offset (within 0.7 dB) by the attenuation due to finite transducer size. Therefore, the overall frequency response of the transducer system used by Goody and Simpson[20] was near unity (within 0.7 dB) for their entire data set. This is discussed further by Goody.[16]

B. Data Uncertainty

The reported uncertainty for each of the data sets is within 1 dB or less. However, the maximum high-frequency (Corcos[38]) correction applied is +17 dB, and examination of Figs. 1 and 2 reveal that the scatter among the data sets is greater than 1 dB. Given the demonstrated ability of the table provide by Corcos[38] to recover the true p spectrum,[21,42–44] the scatter among the data sets determines the uncertainty of spectral estimates predicted using the present model, which is approximately ± 4 dB.

III. New Model

The present empirical model of the p spectrum is a modified form of the Chase–Howe model [Eq. (1)]. When compared to the experimental data surveyed presently, the spectral levels of the Chase–Howe model are low at low frequencies and do not decay as rapidly at high frequencies (Fig. 3). To agree better with the experimental data, Eq. (1) was modified with the following considerations in mind:

1) A term was added to the denominator so that spectral levels decay as ω^{-5} as $\omega \to \infty$.

2) The exponents in the denominator were changed to better agree with the measured p spectral behavior at middle frequencies (the overlap range).

3) A multiplicative constant was added to the model function to raise the spectral levels at all frequencies so that they better agree with the experimental data.

4) The Reynolds number trends that exist in the data are accurately reflected.

A functional form, which incorporates the preceding considerations, is

$$\frac{\Phi(\omega)U_e}{\tau_w^2\delta} = \frac{C_2(\omega\delta/U_e)^2}{\left[(\omega\delta/U_e)^{0.75} + C_1\right]^{3.7} + [C_3(\omega\delta/U_e)]^7} \qquad (2)$$

where C_1, C_2, and/or C_3 vary with Reynolds number. Equation (2) increases as ω^2 at the lowest frequencies, decays as approximately $\omega^{-0.7}$ at middle frequencies (overlap range), and decays as ω^{-5} at the highest frequencies. The ratio of C_1 to C_3 determines the size of the overlap range ($\omega^{-0.7}$ decay, which does not exist beneath low Reynolds number flows). The model parameters (C_1,C_2, and C_3) were determined based on the following three postulates.

First, the p spectrum collapses to a universal curve at low frequencies when normalized using τ_w as the pressure scale and δ/U_e as the timescale, independent of Reynolds number (Fig. 2). Normalizing the p spectra on Q_e only collapses the experimental data at the lowest frequencies ($\omega\delta/U_e < 0.3$, Fig. 4). Only the measurements of Farabee and Casarella[12] have a significant number of data points at frequencies at which Q_e collapse the p spectra. The p spectra collapse over a larger frequency range ($\omega\delta/U_e < 10$) when normalized using τ_w. Therefore, τ_w was used in the present model as the low-frequency pressure scale. The low-frequency timescale uses δ rather than δ^* because the largest coherent structures are of order δ. The ratio δ^*/δ approaches zero as the Reynolds number approaches infinity, and so δ and δ^* are not equivalent as outer-layer length scales.[11] Goody[16] showed that the timescales δ^*/U_e, δ/U_e, δ^*/u_τ, and δ/u_τ collapse experimental p spectra at low frequencies over a large range of Reynolds numbers ($1.4 \times 10^3 < Re_\theta < 2.34 \times 10^4$) as long as τ_w is used as the pressure scale.

Second, the p spectrum collapses to a universal curve at high frequencies when normalized using τ_w as the pressure scale and ν/u_τ^2 as the timescale, independent of Reynolds number (Fig. 1).

Third, the only effect of Reynolds number on the shape of the p spectrum is to increase the size of the overlap range.

The first postulate sets the value of C_1 and C_2. The variation of C_3 with Reynolds number was determined using the second postulate. The goal was to, approximately, express Φ as a $f(\omega\delta/U_e)$ at low frequencies and as $f\ (\omega\nu/u_\tau^2)$ at the highest frequencies. This was approximated using the ratio of the outer-layer-to-inner-layer timescale:

$$(\delta/U_e)\Big/\left(\nu\Big/u_\tau^2\right) = u_\tau^2\delta\Big/U_e\nu = (u_\tau/U_e)(u_\tau\delta/\nu)$$
$$= (u_\tau\delta/\nu)\sqrt{C_f/2} \equiv R_T \tag{3}$$

As R_T increases, the low-frequency, outer-layer-scaled frequency range moves away from the high-frequency, inner-layer-scaled frequency range and the size of the overlap range increases. Thus, following the third postulate, it is R_T, rather than the Reynolds number, that characterizes what is commonly called the Reynolds number effect on the p spectrum.

The model satisfies the first two postulates quantitatively at $\omega\delta/U_e \approx 1.4$ as

$$\left[10\log_{10}\left(\frac{\Phi(\omega)U_e}{\tau_w^2\delta}\right)\right]_{\max} \approx -1.6\,\text{dB}$$

and at $\omega\nu/u_\tau^2 = 2$ as

$$\left[10\log_{10}\left(\frac{\Phi(\omega)u_\tau^2}{\tau_w^2\nu}\right)\right] = -13.5\,\text{dB}$$

using the model parameters

$$C_1 = 0.5, \qquad C_2 = 3.0, \qquad C_3 = 1.1R_T^{-0.57} \tag{4}$$

Example comparisons of the model to experimental data are shown in Figs. 5 and 6.

The final form of the empirical model is

$$\frac{\Phi(\omega)U_e}{\tau_w^2\delta} = \frac{3.0(\omega\delta/U_e)^2}{\left[(\omega\delta/U_e)^{0.75}+0.5\right]^{3.7} + \left[\left(1.1R_T^{-0.57}\right)(\omega\delta/U_e)\right]^7} \tag{5}$$

with R_T as defined in Eq. (3). Figures 7 and 8 show the scaling behavior of the present model for $10 \le R_T \le 2000$. Because the model strictly follows to the high-frequency, inner-layer scaling, the model offers a high degree of confidence when extrapolated to flows with a higher Reynolds number than the data sets surveyed presently, as long as the flow is nearly two dimensional. If the flow contains large turbulence intensity in the freestream or the boundary layer is subjected to large pressure gradients, the validity of the scaling rules, which are the basis of the present model, is no longer universal. Additionally, if the boundary flow is highly three dimensional, highly skewed, or separated, the shape of the pressure spectrum will likely be different than the present model. For example, the flow on a moderate-to-high-aspect-ratio airfoil at low angle of attack is nearly two dimensional over most of the airfoil. The pressure gradients are not severe over most of the surface, and the present model works well. However, at higher angle of attack, the pressure gradient is more severe and the boundary layer may separate. The present model will not work well under these conditions. The present model accurately predicts the pressure spectrum beneath quasi-two-dimensional, quasi-zero-pressure-gradient flow. However, care must be exercised when the model is applied to flows that are not strictly two dimensional with zero pressure gradient. The mean square pressure is discussed by Goody.[45]

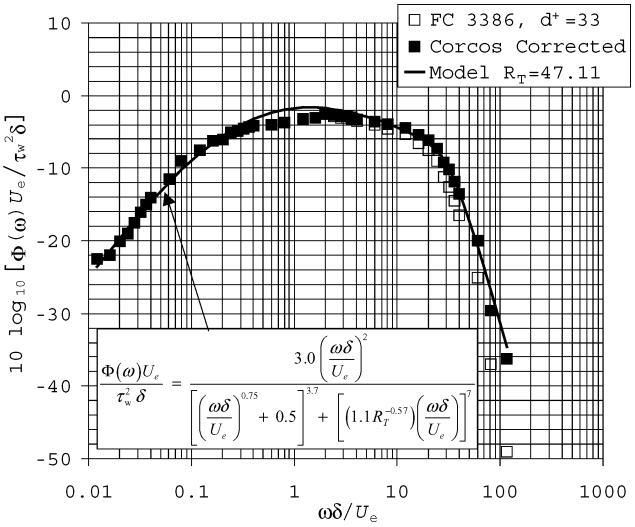

Fig. 5 Comparison of present model with the data of Farabee and Casarella[12]: $d^+ = 33$, $Re_\theta = 3.386 \times 10^3$, and $R_T = 47.11$.

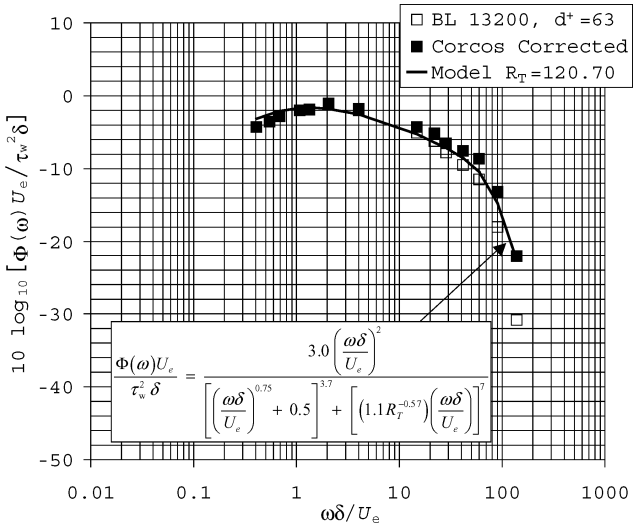

Fig. 6 Comparison of present model with data of Blake[19]: $d^+ = 63$, $Re_\theta = 1.32 \times 10^4$ and $R_T = 120.7$.

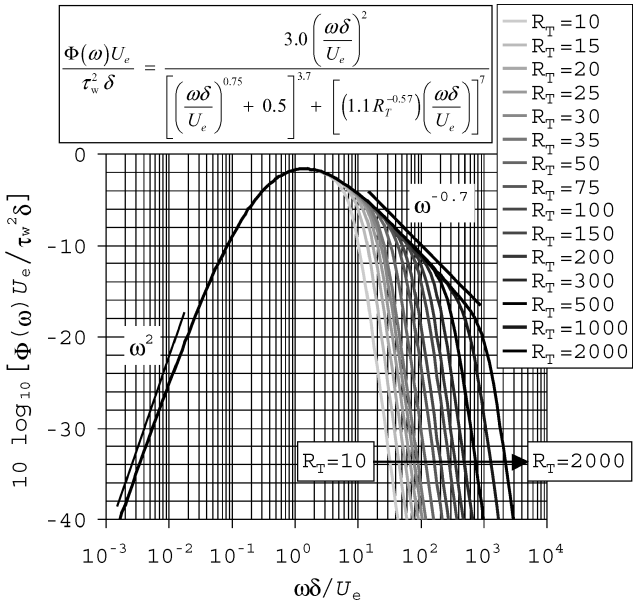

Fig. 7 Model p spectra scaled by outer variables: τ_w as the pressure scale and δ/U_e as timescale.

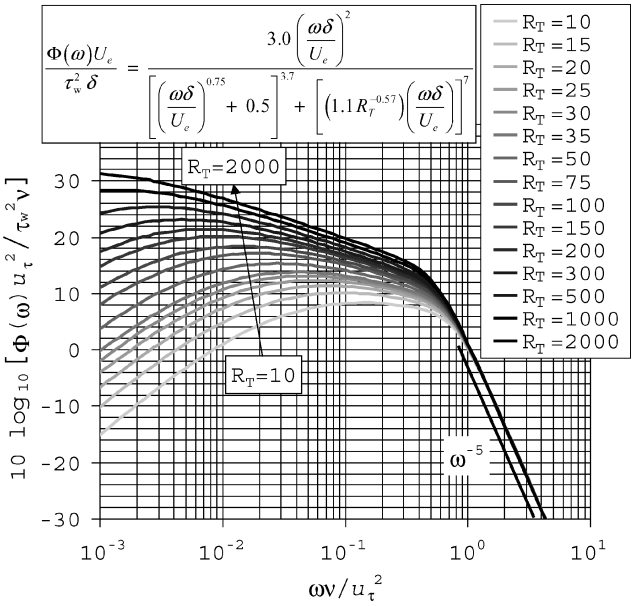

Fig. 8 Model p spectra scaled by inner variables: τ_w as pressure scale and ν/u_τ^2 as timescale.

IV. Relating R_T and Reynolds Number

The timescale R_T is used here to characterize what is commonly known as the Reynolds number effect on the p spectrum. A more accurate term is the effect of the range of relevant scales. The Reynolds number has classically been used in the form

$$Re_L \equiv \frac{\rho U^2}{\mu(U/L)} = \frac{\text{inertial forces}}{\text{viscous forces}} = \frac{U_e L}{\nu} \tag{6}$$

where L is a length scale of the problem, to determine when the Navier–Stokes viscous terms are not significant, in relation to the inertial terms, and can be neglected for given flow conditions. The limit $Re \to \infty$ has also been shown to be a requirement for mathematically rigorous self-similarity.[2] The term Reynolds number has since been commonly used in the literature with a broader, less precise meaning, that is, a measure of how turbulent a flow is, in other words, how far from laminar a flow is. Unfortunately, the mathematical definition of Reynolds number [Eq. (6)] is often retained and used in conjunction with the broader meaning. Equation (6) is often too restrictive to be used in conjunction with the broader meaning.

The distinction between the effect of Reynolds number and the effect of the range of relevant scales is more than a matter of semantics. The two are fundamentally different approaches. The present analysis is a case in point: It links the p spectrum directly to the scales of the flow rather than to the ratio of inertial-to-viscous forces. The analysis is empirical. Any use of boundary-layer scales is empirical in nature: Either a scaling combination collapses the curves, or it does not. Whether or not the curves collapse can only be verified through experiments. The effect of the range of relevant scales is related to the Reynolds number, but the two are not the same. Following the effect of the range of relevant scales approach does not restrict a proposed metric of the boundary layer to the form

$$\text{metric} = (\text{velocity scale})(\text{length scale})/\nu \tag{7}$$

for example, R_T, which is used here.

Because the Reynolds number is more commonly used than R_T to describe a boundary layer, it is useful to show how the two are related. Assume that the velocity profile can be approximated as

$$U/U_e = (y/\delta)^{\frac{1}{7}} \tag{8}$$

and use Blasius's empirical equation for the resistance coefficient in pipe flow in the forms

$$C_f = 0.045\,(\nu/U_e\delta)^{\frac{1}{4}} \tag{9}$$

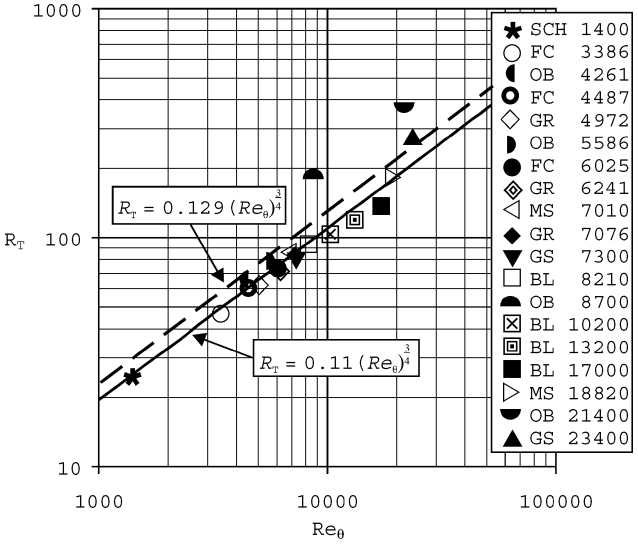

Fig. 9 Timescale ratio R_T as function of Reynolds number Re_θ for experimental data sets.

$$\delta/x = 0.37\,(\nu/U_e x)^{\frac{1}{5}} \tag{10}$$

It can be shown that

$$R_T = 0.129\,(U_e\theta/\nu)^{\frac{3}{4}} \tag{11}$$

$$R_T = 0.0107\,(U_e x/\nu)^{\frac{3}{5}} \tag{12}$$

Figure 9 shows that Eq. (11) agrees well with experimental data; however, there is better agreement when the constant is slightly changed to

$$R_T = 0.11(U_e\theta/\nu)^{\frac{3}{4}} \tag{13}$$

Note that Eqs. (9) and (10) are only strictly valid for low Reynolds number flat-plate boundary layers. However, they are sufficient to show qualitatively how R_T varies with Reynolds number. Qualitatively, the range $10 < R_T < 2000$ corresponds to $408 < Re_\theta < 4.78 \times 10^5$.

V. Conclusions

An empirical spectral model of p has been presented that is similar, in functional form, to the Chase–Howe model and uses the timescale ratio of the boundary layer as a parameter. The model is based on the observed scaling behavior of surface pressure spectra that have been measured by seven research groups and cover a large range of Reynolds number, $1.4 \times 10^3 Re_\theta < 2.34 \times 10^4$. It is proposed that the effect of Reynolds number is more aptly described as the effect of the range of relevant scales. The effect of the range of relevant scales is incorporated into the new model based on the postulate that the only effect of the range of relevant scales is to increase the size of the overlap frequency range. The model can be confidently extrapolated to higher Reynolds number flows because it strictly follows the Reynolds number independent, high-frequency, inner-layer scaling. The p spectral levels predicted by the model compare well to experimental data.

Acknowledgments

This work was sponsored by the Office of Naval Research, L. P. Purtell, Program Monitor.

References

[1]Schetz, J. A., *Boundary Layer Analysis*, Prentice–Hall, Upper Saddle River, NJ, 1993.

[2]Tennekes, H., and Lumley, J. L., *A First Course in Turbulence*, MIT Press, Cambridge, MA, 1972.

[3]Hussain, A. K. M. F., "Coherent Structures and Turbulence," *Journal of Fluid Mechanics*, Vol. 173, 1986, pp. 303–356.

[4]Robinson, S. K., "Coherent Motions in the Turbulent Boundary Layer," *Annual Review of Fluid Mechanics*, Vol. 23, 1991, pp. 601–639.

[5]Panton, R. L., "Scaling Turbulent Wall Layers," *Journal of Fluids Engineering*, Vol. 112, No. 4, 1990, pp. 425–432.

[6]Gad-el-Hak, M., and Bandyopadhyay, P. R., "Reynolds Number Effects in Wall-Bounded Turbulent Flows, "*Applied Mechanics Reviews*, Vol. 47, No. 8, 1994, pp. 307–365.

[7]DeGraaff, D. B., and Eaton, J. K., "Reynolds-Number Scaling of the Flat-plate Turbulent Boundary Layer," *Journal of Fluid Mechanics*, Vol. 422, 2000, pp. 319–346.

[8]Buschmann, M. H., and Gad-el-Hak, M., "The Logarithmic Law In Turbulent Boundary Layers: The Debate Continues," American Society of Mechanical Engineers, Paper CEF-22, Dec. 2001.

[9]Afzal, N., "Millikan's Argument at Moderately Large Reynolds Numbers," *Physics of Fluids*, Vol. 19, No. 4, 1976, pp. 600–602.

[10]Blake, W. K., *Mechanics of Flow-Induced Sound and Vibration*, Academic Press, NewYork, 1986, Chap. 7.

[11]Keith, W. L., Hurdis, D. A., and Abraham, B. M., "A Comparison of Turbulent Boundary Layer Wall-Pressure Spectra," *Journal of Fluids Engineering*, Vol. 114, No. 3, 1992, pp. 338–347.

[12]Farabee, T. M., and Casarella, M. J., "Spectral Features of Wall Pressure Fluctuations Beneath Turbulent Boundary Layers," *Physics of Fluids A*, Vol. 3, No. 10, 1991, pp. 2410–2420.

[13]Bradshaw, P., "'Inactive' Motion and Pressure Fluctuations in Turbulent Boundary Layers," *Journal of Fluid Mechanics*, Vol. 30, 1967, pp. 241–258.

[14]Olivero-Bally, P., Forestier, B. B., Focquenoy, E., and Olivero, P., "Wall-Pressure Fluctuations *Flow Noise Modeling, Measurement, and Control*, in Natural and Manipulated Turbulent Boundary Layers in Air and Water," ASME FED-Vol. 168, American Society of Mechanical Engineers, Fairfield, NJ, 1993, pp. 63–74.

[15]Gravante, S. P., Naquib, A. M., Wark, C. E., and Nagib, H. M., "Characterization of the Pressure Fluctuations Under a Fully Developed Turbulent Boundary Layer," *AIAA Journal*, Vol. 36, 1998, pp. 1808–1816.

[16]Goody, M. C., "An Experimental Investigation of Pressure Fluctuations in Three-Dimensional Turbulent Boundary Layers," Ph.D. Dissertation, Dept. of Aerospace and Ocean Engineering, Virginia Polytechnic Inst. and State Univ., Blacksburg, VA, Sept. 1999; also available at http://scholar.lib.vt.edu/theses/available/etd-120399-144042/ [cited 3 Dec. 1999].

[17]Panton, R. L., and Linebarger, J. H., "Wall Pressure Spectra Calculations for Equilibrium Boundary Layers," *Journal of Fluid Mechanics*, Vol. 65, 1974, pp. 261–287.

[18]McGrath, B. E., and Simpson, R. L., "Some Features of Surface Pressure Fluctuations in Turbulent Boundary Layers with Zero and Favorable Pressure Gradients," NASA CR-4051, 1987.

[19]Blake, W. K., "Turbulent Boundary-Layer Wall-Pressure Fluctuations on Smooth and Rough Walls," *Journal of Fluid Mechanics*, Vol. 44, Pt. 4, 1970, pp. 637–660.

[20]Goody, M. C., and Simpson, R. L., "Surface Pressure Fluctuations Beneath Two- and Three-Dimensional Turbulent Boundary Layers," *AIAA Journal*, Vol. 38, No. 10, 2000, pp. 1822–1831.

[21]Schewe, G., "On the Structure and Resolution of Wall-Pressure Fluctuations Associated with Turbulent Boundary-Layer Flow," *Journal of Fluid Mechanics*, Vol. 134, 1983, pp. 311–328.

[22]Howe, M. S., *Acoustics of Fluid-Structure Interactions*, Cambridge Univ. Press, Cambridge, England, U.K., 1998, p. 208.

[23]Chase, D. M., "Modeling the Wavevector-Frequency Spectrum of Turbulent Boundary Layer Wall Pressure," *Journal of Sound and Vibration*, Vol. 70, No. 1, 1980, pp. 29–67.

[24]Graham, W. R., "A Comparison of Models for the Wavevector-Frequency Spectrum of Turbulent Boundary Layer Pressures," *Journal of Sound and Vibration*, Vol. 206, No. 14, 1997, pp. 541–565.

[25]Corcos, G. M., "The Structure of the Turbulent Pressure Field in Boundary-Layer Flows," *Journal of Fluid Mechanics*, Vol. 18, 1964, pp. 353–378.

[26]Efimtsov, B. M., "Characteristics of the Field of Turbulent Wall Pressure Fluctuations at Large Reynolds Numbers," *Soviet Physics–Acoustics*, Vol. 28, No. 4, 1982, pp. 289–292.

[27]Smol'yakov, A. V., and Tkachenko, V. M., "Model of a Field of Pseudosonic Turbulent Wall Pressures and Experimental Data," *Soviet Physics–Acoustics*, Vol. 37, No. 6, 1991, pp. 627–631.

[28]Ffowcs Williams, J. E., "Boundary-Layer Pressures and the Corcos Model: A Development to Incorporate Low Wavenumber Constraints," *Journal of Fluid Mechanics*, Vol. 125, 1982, pp. 9–25.

[29]Hwang, Y. F., and Geib, F. E., "Estimation of the Wavevector-Frequency Spectrum of Turbulent Boundary Layer Wall Pressure by Multiple Linear Regression," *Journal of Vibration, Acoustics, Stress and Reliability in Design*, Vol. 108, No. 3, 1986, pp. 334–342.

[30]Witting, J. M., "A Spectral Model of Pressure Fluctuations at a Rigid Wall Bounding an Incompressible Fluid, Based on Turbulent Structures in the Boundary Layer," *Noise Control Engineering Journal*, Vol. 26, No. 1, 1986, pp. 28–43.

[31]Panton, R. L., and Robert, G., "The Wavenumber-Phase Velocity Representation for the Turbulent Wall-Pressure Spectrum," *Journal of Fluids Engineering*, Vol. 116, No. 3, 1994, pp. 477–483.

[32]Lighthill, M. J., "On Sound Generated Aerodynamically: I. General Theory," *Proceedings of the Royal Society of London, Series A: Mathematical and Physical Sciences*, Vol. 211, No. 1107, 1952, pp. 564–587.

[33]Lighthill, M. J., "On Sound Generated Aerodynamically: II. Turbulence as a Source of Sound," *Proceedings of the Royal Society of London. Series A: Mathematical and Physical Sciences*, Vol. 222, No. 1148, 1954, pp. 1–32.

[34]Kraichnan, R. H., "Pressure Fluctuations in Turbulent Flow over a Flat Plate," *Journal of the Acoustical Society of America*, Vol. 28, No. 3, 1956, pp. 378–390.

[35]Helal, H. M., Casarella, M. J., and Farabee, T. M., "An Application of Noise Cancellation Techniques to the Measurement of Wall Pressure Fluctuations in a Wind Tunnel," *ASME Winter Annual Meeting*, NCA Vol. 5, American Society of Mechanical Engineers, Fairfield, NJ, 1989, pp. 49–59.

[36]Agarwal, N. K., and Simpson, R. L., "A New Technique for Obtaining the Turbulent Pressure Spectrum from the Surface Pressure Spectrum," *Journal of Sound and Vibration*, Vol. 135, No. 2, 1989, pp. 346–350.

[37]Naquib, A. M., Gravante, S. P., and Wark, C. E., "Extraction of Turbulent Wall-Pressure Time-Series using an Optimal Filtering Scheme," *Experiments in Fluids*, Vol. 22, No. 1, 1989, pp. 14–22.

[38]Corcos, G. M., "Resolution of Pressure in Turbulence," *Journal of the Acoustical Society of America*, Vol. 35, No. 2, 1963, pp. 192–199.

[39]Willmarth, W. W., and Roos, F. W., "Resolution and Structure of the Wall Pressure Field Beneath a Turbulent Boundary Layer," *Journal of Fluid Mechanics*, Vol. 22, 1965, pp. 81–94.

[40]White, P. H., "Effect of Transducer Size, Shape, and Surface Sensitivity on the Measurement of Boundary Layer Pressures," *Journal of the Acoustical Society of America*, Vol. 41, No. 5, 1967, pp. 1358–1363.

[41]Chase, D. M., "Turbulent-Boundary-Layer Pressure Fluctuations and Wavenumber Filtering by Nonuniform Spatial Averaging," *Journal of the Acoustical Society of America*, Vol. 46, No. 5, 1969, pp. 1350–1365.

[42]Gilchrist, R. B., and Strawderman, W. A., "Experimental Hydrophone-Size Correction Factor for Boundary-Layer Pressure Fluctuations," *Journal of the Acoustical Society of America*, Vol. 38, 1965, pp. 298–302.

[43]Geib, F. E., "Measurements on the Effect of Transducer Size on the Resolution of Boundary-Layer Pressure Fluctuations," *Journal of the Acoustical Society of America*, Vol. 46, No. 1, 1969, pp. 253–261.

[44]Lueptow, R. M., "Transducer Resolution and the Turbulent Wall Pressure Spectrum," *Journal of the Acoustical Society of America*, Vol. 97, No. 1, 1995, pp. 370–378.

[45]Goody, M. C., "An Empirical Model of Surface-Pressure Fluctuations that Includes Reynolds Number Effects," AIAA Paper 2002-2565, June 2002.

W. J. Devenport
Associate Editor